Search for hadronic transition χ_{cJ}→η_{c}π^{+}π^{-} and observation of χ_{cJ}→KK[over ¯]ππ

M. Ablikim *et al.* (BESIII Collaboration)

Search for hadronic transition $\chi_{cJ} \to \eta_c \pi^+ \pi^-$ and observation of $\chi_{cJ} \to K\bar{K}\pi\pi$

M. Ablikim[1], M. N. Achasov[5], D. J. Ambrose[39], F. F. An[1], Q. An[40], Z. H. An[1], J. Z. Bai[1],

Y. Ban[27], J. Becker[2], J. V. Bennett[17], M. Bertani[18A], J. M. Bian[38], E. Boger[20,a],

O. Bondarenko[21], I. Boyko[20], R. A. Briere[3], V. Bytev[20], X. Cai[1], O. Cakir[35A], A. Calcaterra[18A],

G. F. Cao[1], S. A. Cetin[35B], J. F. Chang[1], G. Chelkov[20,a], G. Chen[1], H. S. Chen[1], J. C. Chen[1],

M. L. Chen[1], S. J. Chen[25], Y. B. Chen[1], H. P. Cheng[14], Y. P. Chu[1], D. Cronin-Hennessy[38],

H. L. Dai[1], J. P. Dai[1], D. Dedovich[20], Z. Y. Deng[1], A. Denig[19], I. Denysenko[20,b],

M. Destefanis[43A,43C], W. M. Ding[29], Y. Ding[23], L. Y. Dong[1], M. Y. Dong[1], S. X. Du[46], J. Fang[1],

S. S. Fang[1], L. Fava[43B,43C], F. Feldbauer[2], C. Q. Feng[40], R. B. Ferroli[18A], C. D. Fu[1], J. L. Fu[25],

Y. Gao[34], C. Geng[40], K. Goetzen[7], W. X. Gong[1], W. Gradl[19], M. Greco[43A,43C], M. H. Gu[1],

Y. T. Gu[9], Y. H. Guan[6], A. Q. Guo[26], L. B. Guo[24], Y.P. Guo[26], Y. L. Han[1], F. A. Harris[37],

K. L. He[1], M. He[1], Z. Y. He[26], T. Held[2], Y. K. Heng[1], Z. L. Hou[1], H. M. Hu[1], J. F. Hu[6], T. Hu[1],

G. M. Huang[15], J. S. Huang[12], X. T. Huang[29], Y. P. Huang[1], T. Hussain[42], C. S. Ji[40], Q. Ji[1],

X. B. Ji[1], X. L. Ji[1], L. L. Jiang[1], X. S. Jiang[1], J. B. Jiao[29], Z. Jiao[14], D. P. Jin[1], S. Jin[1],

F. F. Jing[34], N. Kalantar-Nayestanaki[21], M. Kavatsyuk[21], W. Kuehn[36], W. Lai[1], J. S. Lange[36],

C. H. Li[1], Cheng Li[40], Cui Li[40], D. M. Li[46], F. Li[1], G. Li[1], H. B. Li[1], J. C. Li[1], K. Li[10], Lei Li[1],

Q. J. Li[1], S. L. Li[1], W. D. Li[1], W. G. Li[1], X. L. Li[29], X. N. Li[1], X. Q. Li[26], X. R. Li[28], Z. B. Li[33],

H. Liang[40], Y. F. Liang[31], Y. T. Liang[36], G. R. Liao[34], X. T. Liao[1], B. J. Liu[1], C. L. Liu[3],

C. X. Liu[1], C. Y. Liu[1], F. H. Liu[30], Fang Liu[1], Feng Liu[15], H. Liu[1], H. B. Liu[6], H. H. Liu[13],

H. M. Liu[1], H. W. Liu[1], J. P. Liu[44], K. Y. Liu[23], Kai Liu[6], P. L. Liu[29], Q. Liu[6], S. B. Liu[40],

X. Liu[22], X. H. Liu[1], Y. B. Liu[26], Z. A. Liu[1], Zhiqiang Liu[1], Zhiqing Liu[1], H. Loehner[21],

G. R. Lu[12], H. J. Lu[14], J. G. Lu[1], Q. W. Lu[30], X. R. Lu[6], Y. P. Lu[1], C. L. Luo[24], M. X. Luo[45],

T. Luo[37], X. L. Luo[1], M. Lv[1], C. L. Ma[6], F. C. Ma[23], H. L. Ma[1], Q. M. Ma[1], S. Ma[1], T. Ma[1],

X. Y. Ma[1], Y. Ma[11], F. E. Maas[11], M. Maggiora[43A,43C], Q. A. Malik[42], Y. J. Mao[27], Z. P. Mao[1],

J. G. Messchendorp[21], J. Min[1], T. J. Min[1], R. E. Mitchell[17], X. H. Mo[1], C. Morales

Morales[11], C. Motzko[2], N. Yu. Muchnoi[5], H. Muramatsu[39], Y. Nefedov[20], C. Nicholson[6],

I. B. Nikolaev[5], Z. Ning[1], S. L. Olsen[28], Q. Ouyang[1], S. Pacetti[18B], J. W. Park[28], M. Pelizaeus[37],

H. P. Peng[40], K. Peters[7], J. L. Ping[24], R. G. Ping[1], R. Poling[38], E. Prencipe[19], M. Qi[25],

S. Qian[1], C. F. Qiao[6], X. S. Qin[1], Y. Qin[27], Z. H. Qin[1], J. F. Qiu[1], K. H. Rashid[42], G. Rong[1],

X. D. Ruan[9], A. Sarantsev[20,c], B. D. Schaefer[17], J. Schulze[2], M. Shao[40], C. P. Shen[37,d],

X. Y. Shen[1], H. Y. Sheng[1], M. R. Shepherd[17], W. M. Song[1], X. Y. Song[1], S. Spataro[43A,43C],

B. Spruck[36], D. H. Sun[1], G. X. Sun[1], J. F. Sun[12], S. S. Sun[1], Y. J. Sun[40], Y. Z. Sun[1], Z. J. Sun[1],

Z. T. Sun[40], C. J. Tang[31], X. Tang[1], I. Tapan[35C], E. H. Thorndike[39], D. Toth[38], M. Ullrich[36],

G. S. Varner[37], B. Wang[9], B. Q. Wang[27], K. Wang[1], L. L. Wang[4], L. S. Wang[1], M. Wang[29],

P. Wang[1], P. L. Wang[1], Q. Wang[1], Q. J. Wang[1], S. G. Wang[27], X. L. Wang[40], Y. D. Wang[40],

Y. F. Wang[1], Y. Q. Wang[29], Z. Wang[1], Z. G. Wang[1], Z. Y. Wang[1], D. H. Wei[8], P. Weidenkaff[19],

Q. G. Wen[40], S. P. Wen[1], M. Werner[36], U. Wiedner[2], L. H. Wu[1], N. Wu[1], S. X. Wu[40],

W. Wu[26], Z. Wu[1], L. G. Xia[34], Z. J. Xiao[24], Y. G. Xie[1], Q. L. Xiu[1], G. F. Xu[1], G. M. Xu[27],

H. Xu[1], Q. J. Xu[10], X. P. Xu[32], Z. R. Xu[40], F. Xue[15], Z. Xue[1], L. Yan[40], W. B. Yan[40],

Y. H. Yan[16], H. X. Yang[1], Y. Yang[15], Y. X. Yang[8], H. Ye[1], M. Ye[1], M. H. Ye[4], B. X. Yu[1],

C. X. Yu[26], J. S. Yu[22], S. P. Yu[29], C. Z. Yuan[1], Y. Yuan[1], A. A. Zafar[42], A. Zallo[18A], Y. Zeng[16],

B. X. Zhang[1], B. Y. Zhang[1], C. C. Zhang[1], D. H. Zhang[1], H. H. Zhang[33], H. Y. Zhang[1],

J. Q. Zhang[1], J. W. Zhang[1], J. Y. Zhang[1], J. Z. Zhang[1], S. H. Zhang[1], X. J. Zhang[1],

X. Y. Zhang[29], Y. Zhang[1], Y. H. Zhang[1], Y. S. Zhang[9], Z. P. Zhang[40], Z. Y. Zhang[44], G. Zhao[1],

H. S. Zhao[1], J. W. Zhao[1], K. X. Zhao[24], Lei Zhao[40], Ling Zhao[1], M. G. Zhao[26], Q. Zhao[1],

S. J. Zhao[46], T. C. Zhao[1], X. H. Zhao[25], Y. B. Zhao[1], Z. G. Zhao[40], A. Zhemchugov[20,a],

B. Zheng[41], J. P. Zheng[1], Y. H. Zheng[6], B. Zhong[1], J. Zhong[2], L. Zhou[1], X. K. Zhou[6],

X. R. Zhou[40], C. Zhu[1], K. Zhu[1], K. J. Zhu[1], S. H. Zhu[1], X. L. Zhu[34], X. W. Zhu[1],

Y. C. Zhu[40], Y. M. Zhu[26], Y. S. Zhu[1], Z. A. Zhu[1], J. Zhuang[1], B. S. Zou[1], J. H. Zou[1]

(BESIII Collaboration)

[1] *Institute of High Energy Physics, Beijing 100049, P. R. China*

[2] *Bochum Ruhr-University, 44780 Bochum, Germany*

[3] *Carnegie Mellon University, Pittsburgh, PA 15213, USA*

[4] *China Center of Advanced Science and Technology, Beijing 100190, P. R. China*

[5] *G.I. Budker Institute of Nuclear Physics SB RAS (BINP), Novosibirsk 630090, Russia*

[6] *Graduate University of Chinese Academy of Sciences, Beijing 100049, P. R. China*

[7] *GSI Helmholtzcentre for Heavy Ion Research GmbH, D-64291 Darmstadt, Germany*

[8] *Guangxi Normal University, Guilin 541004, P. R. China*

[9] *GuangXi University, Nanning 530004,P.R.China*

[10] *Hangzhou Normal University, Hangzhou 310036, P. R. China*

[11] *Helmholtz Institute Mainz, J.J. Becherweg 45,D 55099 Mainz,Germany*

[12] *Henan Normal University, Xinxiang 453007, P. R. China*

[13] *Henan University of Science and Technology, Luoyang 471003, P. R. China*

[14] *Huangshan College, Huangshan 245000, P. R. China*

[15] *Huazhong Normal University, Wuhan 430079, P. R. China*

[16] *Hunan University, Changsha 410082, P. R. China*

[17] *Indiana University, Bloomington, Indiana 47405, USA*

[18] *(A)INFN Laboratori Nazionali di Frascati, Frascati, Italy;*

(B)INFN and University of Perugia, I-06100, Perugia, Italy

[19] *Johannes Gutenberg University of Mainz,*

Johann-Joachim-Becher-Weg 45, 55099 Mainz, Germany

[20] *Joint Institute for Nuclear Research, 141980 Dubna, Russia*

[21] *KVI/University of Groningen, 9747 AA Groningen, The Netherlands*

[22] *Lanzhou University, Lanzhou 730000, P. R. China*

[23] *Liaoning University, Shenyang 110036, P. R. China*

[24] *Nanjing Normal University, Nanjing 210046, P. R. China*

[25] *Nanjing University, Nanjing 210093, P. R. China*

[26] *Nankai University, Tianjin 300071, P. R. China*

[27] *Peking University, Beijing 100871, P. R. China*

[28] *Seoul National University, Seoul, 151-747 Korea*

[29] *Shandong University, Jinan 250100, P. R. China*

[30] *Shanxi University, Taiyuan 030006, P. R. China*

[31] *Sichuan University, Chengdu 610064, P. R. China*

[32] *Soochow University, Suzhou 215006, P. R. China*

[33] *Sun Yat-Sen University, Guangzhou 510275, P. R. China*

[34] *Tsinghua University, Beijing 100084, P. R. China*

[35] *(A)Ankara University, Ankara, Turkey; (B)Dogus University,*

Istanbul, Turkey; (C)Uludag University, Bursa, Turkey

[36] *Universitaet Giessen, 35392 Giessen, Germany*

[37] *University of Hawaii, Honolulu, Hawaii 96822, USA*

[38] *University of Minnesota, Minneapolis, MN 55455, USA*

[39] *University of Rochester, Rochester, New York 14627, USA*

[40] *University of Science and Technology of China, Hefei 230026, P. R. China*

[41] *University of South China, Hengyang 421001, P. R. China*

[42] *University of the Punjab, Lahore-54590, Pakistan*

[43] *(A)University of Turin, Turin, Italy; (B)University of Eastern Piedmont, Alessandria, Italy; (C)INFN, Turin, Italy*

[44] *Wuhan University, Wuhan 430072, P. R. China*

[45] *Zhejiang University, Hangzhou 310027, P. R. China*

[46] *Zhengzhou University, Zhengzhou 450001, P. R. China*

[a] *also at the Moscow Institute of Physics and Technology, Moscow, Russia*

[b] *on leave from the Bogolyubov Institute for Theoretical Physics, Kiev, Ukraine*

[c] *also at the PNPI, Gatchina, Russia*

[d] *now at Nagoya University, Nagoya, Japan*

Abstract

Hadronic transitions of $\chi_{cJ} \to \eta_c \pi^+ \pi^-$ ($J = 0$, 1, 2) are searched for using a sample of 1.06×10^8 $\psi(3686)$ events collected with the BESIII detector at the BEPCII storage ring. The η_c is reconstructed with $K_S^0 K^\pm \pi^\mp$ and $K^+ K^- \pi^0$ final states. No signals are observed in any of the three χ_{cJ} states in either η_c decay mode. At the 90% confidence level, the upper limits are determined to be $\mathcal{B}(\chi_{c0} \to \eta_c \pi^+ \pi^-) < 0.07\%$, $\mathcal{B}(\chi_{c1} \to \eta_c \pi^+ \pi^-) < 0.32\%$, and $\mathcal{B}(\chi_{c2} \to \eta_c \pi^+ \pi^-) < 0.54\%$. The upper limit of $\mathcal{B}(\chi_{c1} \to \eta_c \pi^+ \pi^-)$ is lower than the existing theoretical prediction by almost an order of magnitude. The branching fractions of $\chi_{cJ} \to K_S^0 K^\pm \pi^\mp \pi^+ \pi^-$, $K^+ K^- \pi^+ \pi^- \pi^0$, $\omega K^+ K^-$ and $\phi \pi^+ \pi^- \pi^0$ ($J = 0$, 1, 2) are measured for the first time.

PACS numbers: 13.20.Gd, 13.25.Gv, 14.40.Pq

I. INTRODUCTION

Heavy quarkonia, both $c\bar{c}$ and $b\bar{b}$ bound states, have provided good laboratories for the study of the strong interaction [1, 2]. For the hadronic transitions between the heavy quarkonium states, Yan [3] characterized it as the emission of two soft gluons from the heavy quarks and the conversion of gluons into light hadrons. Based on this scheme, a series of decay rates, such as the E1-E1 hadronic transition, E1-M1 hadronic transition, M1-M1 hadronic transition have been calculated [4, 5]. It has been shown that the multipole expansion can make quite successful predictions for many hadronic transitions between the heavy quarkonia [1, 6]. However, most of these studies are for the transitions among the $^3S_1$ states; the hadronic transitions of ^3P_J states are seldom explored. Using a sample of $\Upsilon(3S)$, CLEO measured for the first time the transition rate of P-wave bottomonium $\chi_{bJ}(2P) \to \chi_{bJ}(1P)\pi\pi$ [7], and the results are consistent with the theoretical predictions [5]. For the hadronic transition of the P-wave charmonium states, there is only an upper limit of 2.2% at the 90% confidence level (C.L.) on the $\chi_{c2} \to \eta_c\pi^+\pi^-$ transition rate recently reported by the BaBar experiment [8]. The process $\chi_{c1} \to \eta_c\pi\pi$, which is dominated by an E1-M1 transition, is calculated in the multipole expansion formalism, and a transition rate $\mathcal{B}(\chi_{c1} \to \eta_c\pi\pi) = (2.72 \pm 0.39)\%$ is predicted [9], while the process $\chi_{c0} \to \eta_c\pi^+\pi^-$ is suppressed by spin-parity conservation.

In this article, we search for $\chi_{cJ} \to \eta_c\pi^+\pi^-$ with η_c decays into $K_S^0 K^\pm\pi^\mp$ and $K^+K^-\pi^0$, where the K_S^0 is reconstructed in $\pi^+\pi^-$ and π^0 in $\gamma\gamma$ final states. We also report the first measurement of the branching fractions of $\chi_{cJ} \to K_S^0 K^\pm\pi^\mp\pi^+\pi^-$, $K^+K^-\pi^+\pi^-\pi^0$, ωK^+K^-, and $\phi\pi^+\pi^-\pi^0$. Here the χ_{cJ} originates from the E1 transition $\psi(3686) \to \gamma\chi_{cJ}$.

II. THE EXPERIMENT AND DATA SETS

The data sample for this analysis consists of 1.06×10^8 events produced at the peak of the $\psi(3686)$ resonance [10]; an additional 42 pb^{-1} of data were collected at a center-of-mass energy of $\sqrt{s}$=3.65 GeV to determine non-resonant continuum background contributions. The data are accumulated with the BESIII detector operated at the BEPCII e^+e^- collider.

The BESIII detector, described in detail in Ref. [11], has an effective geometrical acceptance of 93% of 4π. It contains a small cell helium-based main drift chamber (MDC) which provides momentum measurements of charged particles; a time-of-flight system (TOF) based

on plastic scintillator which helps to identify charged particles; an electromagnetic calorimeter (EMC) made of CsI (Tl) crystals which is used to measure the energies of photons and provide trigger signals; and a muon system (MUC) made of Resistive Plate Chambers (RPC). The resolution of the charged particles is 0.5% at 1 GeV/c in a 1 Tesla magnetic field. The energy loss (dE/dx) measurement provided by the MDC has a resolution better than 6% for electrons from Bhabha scattering. The photon energy resolution can reach 2.5% (5%) at 1 GeV in the barrel (endcaps) of the EMC. And the time resolution of TOF is 80 ps in the barrel and 110 ps in the endcaps.

Monte Carlo (MC) simulated events are used to determine the detection efficiency, optimize the selection criteria, and study the possible backgrounds. The simulation of the BESIII detector is GEANT4 [12] based, where the interactions of the particles with the detector material are simulated. The $\psi(3686)$ resonance is produced with KKMC [13], while the subsequent decays are generated with EvtGen [14]. The study of the background is based on a sample of 10^8 $\psi(3686)$ inclusive decays which are generated with known branching fractions taken from the Particle Data Group (PDG) [15], or with LUNDCHARM [16] for the unmeasured decays.

III. EVENT SELECTION

A charged track should have good quality in the track fitting and be within the angle coverage of the MDC, $|\cos\theta| < 0.93$. Each charged track (excludes those from K_S^0 decays) is required to be within 1 cm of the e^+e^- annihilation interaction point (IP) transverse to the beam line and within 10 cm of the IP along the beam axis. Charged-particle identification (PID) is based on combining the dE/dx and TOF information in the variable $\chi^2_{\mathrm{PID}}(i) = \left(\frac{dE/dx_{\mathrm{measured}}-dE/dx_{\mathrm{expected}}}{\sigma_{dE/dx}}\right)^2 + \left(\frac{\mathrm{TOF}_{\mathrm{measured}}-\mathrm{TOF}_{\mathrm{expected}}}{\sigma_{\mathrm{TOF}}}\right)^2$. The values $\chi^2_{\mathrm{PID}}(i)$ and the corresponding confidence levels $\mathrm{Prob}_{\mathrm{PID}}(i)$ are calculated for each charged track for each particle hypothesis i (pion, kaon, or proton).

Photons are reconstructed from isolated showers in the EMC which are at least 20 degrees away from any of the charged tracks. In order to improve the reconstruction efficiency and the energy resolution, the energy deposited in the nearby TOF counter is included. Photon candidates are required to have the energy greater than 25 MeV in the EMC barrel region ($|\cos\theta| < 0.8$), while in the EMC endcap region ($0.86 < |\cos\theta| < 0.92$), the energy threshold

requirement is increased to 50 MeV. EMC timing requirements are used to suppress noise and energy deposits unrelated to the event.

K_S^0 candidates are reconstructed from secondary vertex fits to all the charged-track pairs in an event (assume the tracks to be π). The combination with the best fit quality is kept, and the K_S^0 candidate must have an invariant mass within 7 MeV/c^2 of the K_S^0 nominal mass and the secondary vertex be at least 0.5 cm away from the IP. The reconstructed K_S^0 information is used as input for the subsequent kinematic fit. The π^0 candidates are reconstructed from pairs of photons with an invariant mass in the range $0.120 \, \mathrm{GeV}/c^2 < M(\gamma\gamma) < 0.145 \, \mathrm{GeV}/c^2$.

In selecting $\psi(3686) \to \gamma K_S^0 K^{\pm}\pi^{\mp}\pi^+\pi^-$, a candidate event should have at least six charged tracks and at least one photon. After K_S^0 selection, the event should have exactly four additional charged tracks with zero net charge. While in selecting $\psi(3686) \to \gamma K^+K^-\pi^+\pi^-\pi^0$, a candidate event should have four charged tracks with zero net charge and at least three photons. The $\gamma K_S^0 K^{\pm}\pi^{\mp}\pi^+\pi^-$ ($\gamma K^+K^-\pi^+\pi^-\pi^0$) candidate is then subjected to a four-constraint (4C) kinematic fit provided by four-momentum conservation to reduce background and improve the mass resolution. To determine the species of the final state particles and select the best photons when additional photons (and π^0 candidates) are found in an event, the combination with the minimum value of χ^2 is retained. Here $\chi^2 = \chi^2_{4\mathrm{C}} + \sum_{j=1}^{4} \chi^2_{\mathrm{PID}}(j)$ is the sum of the chi-square from the 4C kinematic fit ($\chi^2_{4\mathrm{C}}$) and that of PID. Events with $\chi^2_{4\mathrm{C}} < 50$ are kept as $\gamma K_S^0 K^{\pm}\pi^{\mp}\pi^+\pi^-$ ($\gamma K^+K^-\pi^+\pi^-\pi^0$) candidates.

There is substantial background from $\psi(3686) \to X + J/\psi$ decays. The $\psi(3686) \to \pi^+\pi^-J/\psi$ events are removed by requiring the recoil mass of any $\pi^+\pi^-$ pair to be outside of a $\pm 3\sigma$ window around the J/ψ nominal mass, where σ is the resolution of the $\pi^+\pi^-$ recoil mass. The $\psi(3686) \to \eta J/\psi$, $\eta \to \gamma\pi^+\pi^-$ events are rejected if $0.535 \, \mathrm{GeV}/c^2 < M(\gamma\pi^+\pi^-) < 0.555 \, \mathrm{GeV}/c^2$. To reject background with one more photon than the signal events ($\gamma\gamma K_S^0 K^{\pm}\pi^{\mp}\pi^+\pi^-$ or $\gamma\gamma K^+K^-\pi^+\pi^-\pi^0$), $\chi^2_{4\mathrm{C}} > 10$ is required when a 4C kinematic fit to $\gamma\gamma K_S^0 K^{\pm}\pi^{\mp}\pi^+\pi^-$ or $\gamma\gamma K^+K^-\pi^+\pi^-\pi^0$ is applied to the event; and to suppress $\psi(3686) \to \pi^0\pi^0 J/\psi$, $J/\psi \to K^+K^-\pi^+\pi^-$ background, $M(K^+K^-\pi^+\pi^-) > 3.125 \, \mathrm{GeV}/c^2$ or $M(K^+K^-\pi^+\pi^-) < 3.095 \, \mathrm{GeV}/c^2$ is required.

In the measurement of $\mathcal{B}(\chi_{cJ} \to K^+K^-\pi^+\pi^-\pi^0)$, the contributions from intermediate states with narrow resonances such as η, ω, and ϕ are excluded. Events from $\chi_{cJ} \to \eta K^+K^-$, $\chi_{cJ} \to \omega K^+K^-$, $\chi_{cJ} \to \phi K^+K^-$, and $\chi_{cJ} \to \phi\pi^+\pi^-\pi^0$ are removed by requiring $|m_{\pi^+\pi^-\pi^0} -$

$m_\eta| > 15$ MeV$/c^2$, $|m_{\pi^+\pi^-\pi^0} - m_\omega| > 40$ MeV$/c^2$, $|m_{\pi^+\pi^-\pi^0} - m_\phi| > 15$ MeV$/c^2$, and $|m_{K^+K^-} - m_\phi| > 15$ MeV$/c^2$. The contribution from $\chi_{cJ} \to \phi\phi$, $\phi \to K^+K^-$, $\phi \to \pi^+\pi^-\pi^0$ events is also removed by these requirements.

In the measurements of $\mathcal{B}(\chi_{cJ} \to \eta_c\pi^+\pi^-)$, $\mathcal{B}(\chi_{cJ} \to \eta K^+K^-)$, $\mathcal{B}(\chi_{cJ} \to \omega K^+K^-)$, $\mathcal{B}(\chi_{cJ} \to \phi K^+K^-)$, and $\mathcal{B}(\chi_{cJ} \to \phi\pi^+\pi^-\pi^0)$, the signal regions of χ_{c0}, χ_{c1}, χ_{c2}, and the mass region of η_c are defined as [3.38, 3.45] GeV$/c^2$, [3.48, 3.54] GeV$/c^2$, [3.54, 3.60] GeV$/c^2$, and [2.70, 3.20] GeV$/c^2$, respectively.

IV. DATA ANALYSIS

A. $\chi_{cJ} \to K_S^0 K^{\pm}\pi^{\mp}\pi^+\pi^-$ and $\chi_{cJ} \to K^+K^-\pi^+\pi^-\pi^0$

After the above selection, the invariant mass distributions of the hadron system are shown in Fig. 1, and clear χ_{cJ} signals are observed with very low background level in the two decay modes.
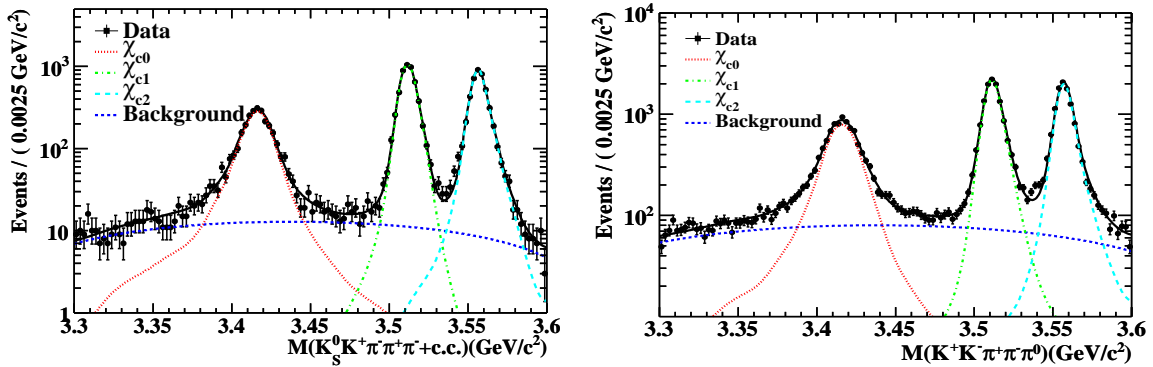
FIG. 1: Invariant mass spectrum of $K_S^0 K^{\pm}\pi^{\mp}\pi^+\pi^-$ (left panel) and $K^+K^-\pi^+\pi^-\pi^0$ (right panel), together with the best fit results. The points with error bars are data, and the solid lines are the total fit results. The χ_{c0}, χ_{c1}, and χ_{c2} signals are shown as dotted lines, dash-dotted lines, and long-dashed lines, respectively; the backgrounds are in dashed lines.

Using the inclusive MC events sample, the potential backgrounds from the $\psi(3686)$ decays which may contaminate $\chi_{cJ} \to K_S^0 K^{\pm}\pi^{\mp}\pi^+\pi^-$ ($\chi_{cJ} \to K^+K^-\pi^+\pi^-\pi^0$) are estimated. Events from $\psi(3686) \to \gamma\chi_{cJ}$, $\chi_{cJ} \to K_S^0 K_S^0 \pi^+\pi^-$ and $\chi_{c0} \to K_S^0 K_S^0 K^+K^-$ ($\psi(3686) \to \gamma\chi_{cJ}$, $\chi_{cJ} \to K_S^0 K^{\pm}\pi^{\mp}\pi^0$) may peak at the signal region, and the contributions

from these peaking backgrounds are estimated using the detection efficiencies determined from the MC simulations and the corresponding branching fractions from previous measurements [15], and then subtracted from the signal yield. These background events after final event selection are listed in Table I and II; the errors in the numbers of events are from the uncertainties of the detection efficiency and branching fractions. The other backgrounds are composed of dozens of decay modes and smoothly distributed in the full mass region ([3.3, 3.6] GeV/c^2); the contribution of this kind of background can be represented by the smooth background term in the fit.

TABLE I: The number of remanent peaking background events ($N_{\text{bkg}}^{\text{peak}}$) in $\chi_{cJ} \to K_S^0 K^\pm \pi^\mp \pi^+ \pi^-$ after final event selection. The branching fractions ($\mathcal{B}$) are taken from PDG [15].

Decay modes	$N_{\text{bkg}}^{\text{peak}}$	$\mathcal{B}$ [15]
$\chi_{c0} \to K_S^0 K_S^0 \pi^+ \pi^-$	4.9 ± 1.4	$(5.8 \pm 1.1) \times 10^{-3}$
$\chi_{c1} \to K_S^0 K_S^0 \pi^+ \pi^-$	0.1 ± 0.1	$(7.2 \pm 3.1) \times 10^{-4}$
$\chi_{c2} \to K_S^0 K_S^0 \pi^+ \pi^-$	0.6 ± 0.3	$(2.4 \pm 0.6) \times 10^{-3}$
$\chi_{c0} \to K_S^0 K_S^0 K^+ K^-$	43 ± 16	$(1.4 \pm 0.5) \times 10^{-3}$

TABLE II: The number of remanent peaking background events ($N_{\text{bkg}}^{\text{peak}}$) in $\chi_{cJ} \to K^+ K^- \pi^+ \pi^- \pi^0$ after final event selection. The branching fractions ($\mathcal{B}$) are taken from PDG [15].

Decay modes	$N_{\text{bkg}}^{\text{peak}}$	$\mathcal{B}$ [15]
$\chi_{c0} \to K_S^0 K^\pm \pi^\mp \pi^0$	124 ± 19	$\frac{1}{2} \times (2.52 \pm 0.34) \times 10^{-2}$
$\chi_{c1} \to K_S^0 K^\pm \pi^\mp \pi^0$	39.0 ± 9.1	$\frac{1}{2} \times (9.0 \pm 1.5) \times 10^{-3}$
$\chi_{c2} \to K_S^0 K^\pm \pi^\mp \pi^0$	52.5 ± 9.3	$\frac{1}{2} \times (1.51 \pm 0.22) \times 10^{-2}$

Data taken at $\sqrt{s} = 3.65$ GeV are used to estimate backgrounds from the continuum process $e^+ e^- \to q\bar{q}$. This kind of background is found to be small and uniformly distributed in the full mass region of interest in both decay modes, so the contribution can be represented by the smooth background term in the fit.

An unbinned maximum likelihood fit is applied to the invariant mass spectrum of
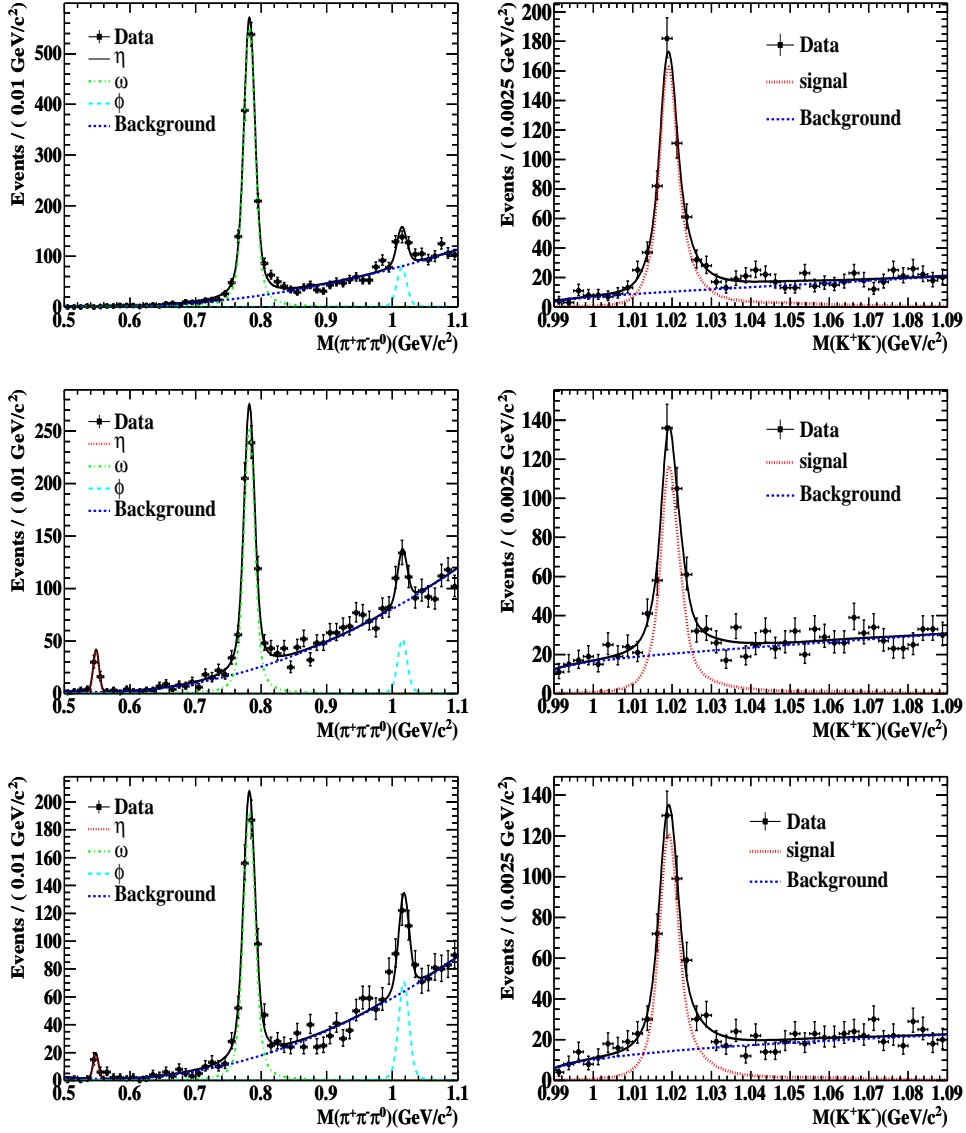
FIG. 2: Fits to the invariant mass spectrum of $\pi^+\pi^-\pi^0$ (left panels) and K^+K^- (right panels) in three χ_{cJ} mass region after $\chi_{cJ} \to \phi\phi$, $\phi \to K^+K^-$, $\phi \to \pi^+\pi^-\pi^0$ were rejected. From top to bottom are in χ_{c0} mass region, χ_{c1} mass region, and χ_{c2} mass region, respectively.

$K_S^0 K^{\pm}\pi^{\mp}\pi^+\pi^-$ ($K^+K^-\pi^+\pi^-\pi^0$) to extract the numbers of χ_{cJ} events in Fig. 1. The χ_{cJ} signals are described by the corresponding MC simulated signal shape convolved with a Gaussian function $G(\mu, \sigma)$ to take into account the difference in the mass scale and the mass resolution between data and MC simulation. The means (μ) and the standard deviations (σ) of the Gaussian functions are floated parameters in the fit. In the generation of the χ_{c0} MC events, the E1 radiative transition factor E_γ^3 is included, where E_γ is the

TABLE III: The number of background events ($N_{\mathrm{bkg}}^{\mathrm{peak}}$) remained in $\chi_{cJ} \to K^+K^-\pi^+\pi^-\pi^0$ from modes with narrow intermediate states. The branching fraction of $\chi_{cJ} \to \phi\phi$ is taken from the BESIII measurement [19] with both statistical and systematic errors; the other branching fractions are measured in this analysis. We also list PDG values [15] in the last column for comparison.

Decay modes	$N_{\mathrm{bkg}}^{\mathrm{peak}}$	Branching fraction	PDG [15] value
$\chi_{c0} \to \eta K^+K^-$	0	forbidden by J^P-conservation	$< 2.3 \times 10^{-4}$
$\chi_{c1} \to \eta K^+K^-$	3.81 ± 0.70	$(3.48 \pm 0.57) \times 10^{-4}$	$(3.3 \pm 1.0) \times 10^{-4}$
$\chi_{c2} \to \eta K^+K^-$	1.90 ± 0.53	$(1.69 \pm 0.45) \times 10^{-4}$	$< 3.5 \times 10^{-4}$
$\chi_{c0} \to \omega K^+K^-$	137 ± 11	$(1.94 \pm 0.06 \pm 0.20) \times 10^{-3}$	-
$\chi_{c1} \to \omega K^+K^-$	69.2 ± 6.2	$(7.82 \pm 0.36 \pm 0.84) \times 10^{-4}$	-
$\chi_{c2} \to \omega K^+K^-$	57.3 ± 5.0	$(7.32 \pm 0.39 \pm 0.78) \times 10^{-4}$	-
$\chi_{c0} \to \phi K^+K^-$	30.4 ± 4.9	$(1.15 \pm 0.17) \times 10^{-3}$	$(0.98 \pm 0.25) \times 10^{-3}$
$\chi_{c1} \to \phi K^+K^-$	17.6 ± 3.8	$(0.67 \pm 0.14) \times 10^{-3}$	$(0.43 \pm 0.16) \times 10^{-3}$
$\chi_{c2} \to \phi K^+K^-$	30.4 ± 5.3	$(1.14 \pm 0.16) \times 10^{-3}$	$(1.55 \pm 0.33) \times 10^{-3}$
$\chi_{c0} \to \phi\pi^+\pi^-\pi^0$	49.6 ± 2.7	$(1.18 \pm 0.07 \pm 0.13) \times 10^{-3}$	-
$\chi_{c1} \to \phi\pi^+\pi^-\pi^0$	28.6 ± 2.0	$(7.54 \pm 0.53 \pm 0.80) \times 10^{-4}$	-
$\chi_{c2} \to \phi\pi^+\pi^-\pi^0$	34.5 ± 2.4	$(9.25 \pm 0.63 \pm 0.97) \times 10^{-4}$	-
$\chi_{c0} \to \phi\phi$	0.97 ± 0.17	$(8.0 \pm 0.3 \pm 0.8) \times 10^{-4}$	$(8.2 \pm 0.8) \times 10^{-4}$
$\chi_{c1} \to \phi\phi$	0.38 ± 0.08	$(4.4 \pm 0.3 \pm 0.5) \times 10^{-4}$	-
$\chi_{c2} \to \phi\phi$	1.03 ± 0.20	$(10.7 \pm 0.3 \pm 1.2) \times 10^{-4}$	$(11.4 \pm 1.2) \times 10^{-4}$

energy of the radiative photon in the $\psi(3686)$ rest frame. To damp the diverging tail due to the E_γ^3 dependence, a damping function $\frac{E_0^2}{E_\gamma E_0 + (E_\gamma - E_0)^2}$ used by KEDR [18] is introduced, where $E_0 = (m_{\psi(3686)}^2 - m_{\chi_{c0}}^2)/2m_{\psi(3686)}$. The backgrounds are described by a second-order Chebyshev polynomial in both decay modes.

The fit to the invariant mass spectrum of $K_S^0 K^\pm \pi^\mp \pi^+ \pi^-$ yields 2837 ± 64, 5180 ± 75, and 4560 ± 71 signal events for χ_{c0}, χ_{c1}, and χ_{c2}, respectively; while the fit to the $K^+K^-\pi^+\pi^-\pi^0$ modes yields 9372 ± 130, 12415 ± 126, and 11366 ± 123 events for χ_{c0}, χ_{c1}, and χ_{c2}, respectively.

In order to estimate the remanent events from $\chi_{cJ} \to \eta K^+K^-$, $\chi_{cJ} \to \omega K^+K^-$, $\chi_{cJ} \to$

$\phi K^+ K^-$, and $\chi_{cJ} \to \phi \pi^+ \pi^- \pi^0$, the branching fractions of these decays are measured using the sample of 1.06×10^8 $\psi(3686)$ events. The identifications of η, ω, and ϕ resonances are similar to those used in Refs. [19, 20]. The fits to the invariant mass spectrum of $\pi^+ \pi^- \pi^0$ and $K^+ K^-$ in the three χ_{cJ} signal regions are shown in Fig. 2. Similar to the χ_{cJ} signals, the η, ω, and ϕ signals are also described with the corresponding MC simulated signal shapes convolved with a Gaussian function. The backgrounds in the fits to the invariant mass spectra of $\pi^+ \pi^- \pi^0$ are described by a second-order Chebyshev polynomial, while those in the fits to the invariant mass spectra of $K^+ K^-$ are described by $(m - m_t)^c \cdot e^{-dm}$, where m_t is the mass threshold of $K^+ K^-$, c and d are free parameters. The results are listed in Table III. The first errors are statistical and the second ones are systematic. The sources of the systematic errors are similar to those in the measurement of $\mathcal{B}(\chi_{cJ} \to K^+ K^- \pi^+ \pi^- \pi^0)$, as will be shown in Sect. V. The branching fractions of $\chi_{cJ} \to \omega K^+ K^-$ and $\chi_{cJ} \to \phi \pi^+ \pi^- \pi^0$ are measured for the first time, and those of other modes from this measurement are consistent within errors with the known PDG values [15] when available. The expected remaining events from these decay channels are also listed in Table III and will be subtracted from the signal yields from the best fits.

B. $\chi_{cJ} \to \eta_c \pi^+ \pi^-$

The invariant mass spectra of $K_S^0 K^\pm \pi^\mp$ $(K^+ K^- \pi^0)$ with $K_S^0 K^\pm \pi^\mp \pi^+ \pi^-$ $(K^+ K^- \pi^+ \pi^- \pi^0)$ in the three χ_{cJ} signal regions are shown in Fig. 3. In both decay modes, there are no significant η_c signal in χ_{c0} and χ_{c1} decay; the η_c signal observed in χ_{c2} decays is found to be mainly from the remaining $\psi(3686) \to \pi^+ \pi^- J/\psi$, $J/\psi \to \gamma \eta_c$, $\eta_c \to K_S^0 K^\pm \pi^\mp$ $(\eta_c \to K^+ K^- \pi^0)$, as described below.

The potential backgrounds from $\psi(3686)$ decays are investigated with the inclusive MC events. The dominant backgrounds are the irreducible $\psi(3686) \to \gamma \chi_{cJ}$, $\chi_{cJ} \to K_S^0 K^\pm \pi^\mp \pi^+ \pi^-$ $(\chi_{cJ} \to K^+ K^- \pi^+ \pi^- \pi^0)$ events. These events have the same final states as the signal events but $K_S^0 K^\pm \pi^\mp$ $(K^+ K^- \pi^0)$ are not from the decay of η_c. In the χ_{c2} signal region, the energy of the transition photon in $J/\psi \to \gamma \eta_c$ in the peaking background mode described above is very close to the energy of the transition photon in $\psi(3686) \to \gamma \chi_{c2}$, and the final states are the same as the signal events. These background cannot be further suppressed without hurting the sensitivity significantly, so we measure its contribution and
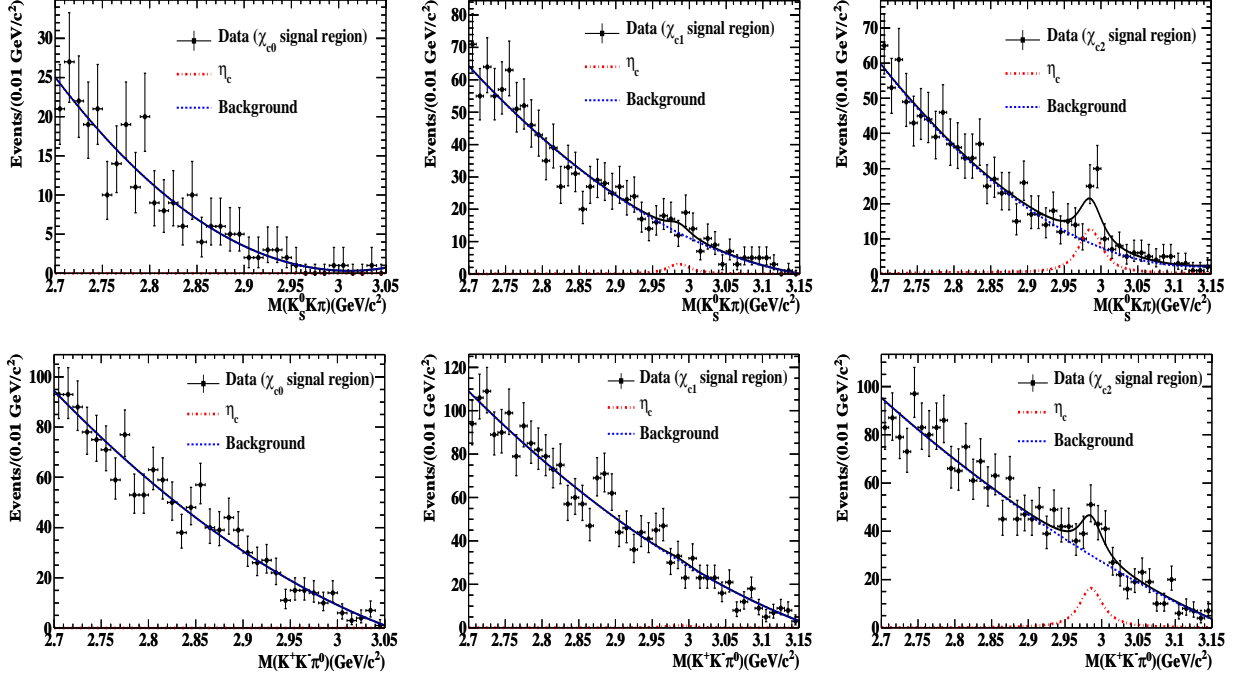
12

FIG. 3: Invariant mass spectra of $K_S^0 K^{\pm} \pi^{\mp}$ (top row) and $K^+ K^- \pi^0$ (bottom row) with $K \bar{K} \pi \pi \pi$ in χ_{c0} (left panel), χ_{c1} (middle panel), and χ_{c2} (right panel) signal regions and the fit results. Dots with error bars are data; the solid lines are the total results from the best fits to the invariant mass spectrum. The η_c signals are shown in dash-dotted lines (in χ_{c2} mass region, the contribution from the peaking background is not removed.); the backgrounds as dashed lines.

subtract it from the signal yield from the fit below. The other backgrounds are composed of dozens of decay channels, each with a small contribution. The dominant backgrounds and the other backgrounds contribute a smooth component in the η_c mass region, so these backgrounds are described by a smooth term in the fit as shown in Fig. 3. In the χ_{c2} case, the peaking background has the same final state and similar kinematics as the signal events, so we use the same line-shape to describe both of them. Data taken at $\sqrt{s} = 3.65$ GeV are used to estimate backgrounds from the continuum process $e^+ e^- \to q\bar{q}$. It is found that this background is small and uniformly distributed in the full mass region in both decay modes, so the contribution is also included in the smooth background term in the fit.

An unbinned maximum likelihood fit is applied to the invariant mass spectra of $K_S^0 K^{\pm} \pi^{\mp}$ ($K^+ K^- \pi^0$) to extract the number of η_c events, as shown in Fig. 3. The η_c signal is described by a MC simulated line shape with the detector resolution included, and the resonance

parameters of η_c are fixed to the latest measurement from the BESIII experiment [17]. The background (except the peaking background in the χ_{c2} signal region) is described with a second-order Chebyshev polynomial in both decay modes in the three χ_{cJ} signal regions.

As there is no significant η_c signal in any of the three χ_{cJ} states in either η_c decay mode, we set upper limits on $\mathcal{B}(\chi_{cJ} \to \eta_c \pi^+ \pi^-)$ using the probability density function (PDF) for the expected number of signal events. In the χ_{c0} and χ_{c1} signal regions, the likelihood distributions of the fit to the invariant mass spectra in Fig. 3 are taken as the PDFs directly. They are obtained by setting the number of η_c signal events from zero up to a very large number. In the χ_{c2} signal region, the likelihood distribution also contains the contribution from the peaking background. Using the known branching fractions [15], the detection efficiency from MC simulation, and the number of $\psi(3686)$ events, the expected peaking background are 45.7 ± 11.6 in $K_S^0 K^{\pm} \pi^{\mp}$ and 34.4 ± 8.7 in $K^+ K^- \pi^0$. Here, the errors include the uncertainties in the detection efficiency and the branching fractions. The PDF of the peaking background is a Gaussian distribution with the mean set to the expected number of events and sigma set to its error. And the PDF of the signal is the distribution of $N_{\text{signal}}^k = N_{\text{fit}}^k - N_{\text{background}}^k$, here N_{fit}^k is a random number generated according to the PDF from the fit, and $N_{\text{background}}^k$ is a random number generated according to the PDF of the peaking background with the requirement $N_{\text{background}}^k \leq N_{\text{fit}}^k$. The systematic uncertainties are considered by smearing the PDF in each decay with a Gaussian function. The upper limit on the number of events at the 90% C.L. is defined as N^{up}, corresponding to the number of events at 90% of the integral of the smeared PDF.

V. SYSTEMATIC UNCERTAINTIES

The systematic uncertainties in the measurement of $\mathcal{B}(\chi_{cJ} \to K\bar{K}\pi\pi\pi)$ and $\mathcal{B}(\chi_{cJ} \to \eta_c \pi^+ \pi^-)$ are summarized in Tables IV and V, respectively. While some common systematics of the BESIII experiment are mentioned briefly below and described elsewhere, the other specific systematic errors are described in detail in the following subsections. The systematic errors related to the MDC tracking (2% per track for those from IP), photon reconstruction (1% per photon), and π^0 reconstruction (1%) are estimated with control samples [20, 21]; the errors in the branching fractions of $\psi(3686) \to \gamma\chi_{cJ}$ and $\eta_c \to K\bar{K}\pi$ are taken from the PDG [15] and are propagated to the χ_{cJ} branching fraction measurement. There is an

14

overall 4% uncertainty in the branching fraction associated with the determination of the number of $\psi(3686)$ events in our data sample [10].

Due to the limited statistics of the MC samples used, a 2% uncertainty is taken for each decay. In each measurement, the bias of the fit is studied with both the toy MC experiments generated with the PDF used in the fit and the input/output check on the number of events in the inclusive MC samples. No bias is found in these tests. For the measurement of the hadronic transition $\chi_{cJ} \to \eta_c \pi^+ \pi^-$, the expected upper limits on the signal events are determined using the toy MC experiments. For each toy MC experiment, the method of the upper limit calculation performed on data is repeated, and the median of the upper limit distribution for all the toy MC experiments is taken as the expected limit, as listed in Table VIII.

TABLE IV: Systematic errors (in %) of $\mathcal{B}(\chi_{cJ} \to K_S^0 K^\pm \pi^\mp \pi^+ \pi^-)$ and $\mathcal{B}(\chi_{cJ} \to K^+ K^- \pi^+ \pi^- \pi^0)$.

Sources	$K_S^0 K^\pm \pi^\mp \pi^+ \pi^-$			$K^+ K^- \pi^+ \pi^- \pi^0$		
	χ_{c0}	χ_{c1}	χ_{c2}	χ_{c0}	χ_{c1}	χ_{c2}
MDC tracking		8.0			8.0	
Photon reconstruction		1.0			3.0	
MC statistics	1.1	1.4	1.5	1.0	1.4	1.4
K_S^0 reconstruction	1.4	1.6	1.7	–	–	–
π^0 reconstruction	–	–	–		1.0	
Kinematic fit	1.5	1.9	1.7	0.4	0.4	0.2
Damping function	0.5	0.1	0.1	0.4	0.1	0.1
Intermediate states	1.0	1.0	1.0	4.0	4.0	4.0
Fitting range	1.0	0.4	0.2	0.4	0.4	0.7
Background shape	1.4	0.7	0.6	1.3	0.7	0.4
$\mathcal{B}(\psi(3686) \to \gamma\chi_{cJ})$	3.2	4.4	3.9	3.2	4.4	3.9
Number of $\psi(3686)$ events		4.0			4.0	
Total	10.1	10.5	10.3	10.9	11.3	11.2

TABLE V: Systematic errors (in %) of $\mathcal{B}(\chi_{cJ} \to \eta_c \pi^+ \pi^-)$ in $\eta_c \to K_S^0 K^\pm \pi^\mp$ and $\eta_c \to K^+ K^- \pi^0$ decay modes.

Sources	$\eta_c \to K_S^0 K^\pm \pi^\mp$			$\eta_c \to K^+ K^- \pi^0$		
	χ_{c0}	χ_{c1}	χ_{c2}	χ_{c0}	χ_{c1}	χ_{c2}
MDC tracking		8.0			8.0	
Photon reconstruction		1.0			3.0	
MC statistics	1.8	1.5	1.6	1.8	1.5	1.7
K_S^0 reconstruction	2.4	2.3	2.2	–	–	–
π^0 reconstruction	–	–	–		1.0	
Kinematic fit	1.5	1.7	1.8	0.9	0.2	0.4
$\mathcal{B}(\psi(3686) \to \gamma\chi_{cJ})$	3.2	4.4	3.9	3.2	4.4	3.9
$\mathcal{B}(\eta_c \to K\bar{K}\pi)$		8.4			8.4	
Number of $\psi(3686)$ events		4.0			4.0	
Total	13.2	13.5	13.4	13.2	13.5	13.4

A. K_S^0 reconstruction

The uncertainty in the K_S^0 reconstruction arises from three parts: the geometric acceptance, the tracking efficiency, and the efficiency of K_S^0 selection. The first part is estimated using MC simulation, and the other two are studied using $J/\psi \to K^{*\pm} K^\mp$, $K^{*\pm} \to K^0 \pi^\pm$. By selecting a pair of $K^\pm \pi^\mp$, the recoil mass spectrum shows a clear K^0 signal. The efficiency of K_S^0 reconstruction is calculated with $\frac{n_1}{\mathcal{B}(K_S^0 \to \pi^+\pi^-) \times (n_1+n_2)/2}$, where n_1 is the number of K^0 obtained from a fit to the $K^\pm \pi^\mp$ recoiling mass when there is a K_S^0 reconstructed in the recoil side that satisfies the K_S^0 selection, and n_2 is the number of K^0 from fitting to the $K^\pm \pi^\mp$ recoiling mass spectrum when no K_S^0 candidate satisfies the K_S^0 selection. The difference in the efficiency of K_S^0 reconstruction ($\varepsilon^{\mathrm{data}}/\varepsilon^{\mathrm{MC}} - 1$) as a function of K_S^0 momentum is shown in Fig. 4. The difference in the K_S^0 reconstruction between data and MC simulation is fitted with a linear function of the K_S^0 momentum as shown in Fig. 4 together with the $\pm 1\sigma$ envelops. Since the difference between data and MC is significant, we do a correction to the signal MC according to the momentum of K_S^0, and the uncertainty of this correction

16

is taken as the systematic error.

The systematic errors in $\mathcal{B}(\chi_{cJ} \to K_S^0 K^{\pm} \pi^{\mp} \pi^+ \pi^-)$ are found to be 1.4%, 1.6%, and 1.7%, for $J = 0$, 1, and 2, respectively; while for $\mathcal{B}(\chi_{cJ} \to \eta_c \pi^+ \pi^-)$, they are 2.4%, 2.3%, and 2.2% for χ_{c0}, χ_{c1}, and χ_{c2}, respectively.
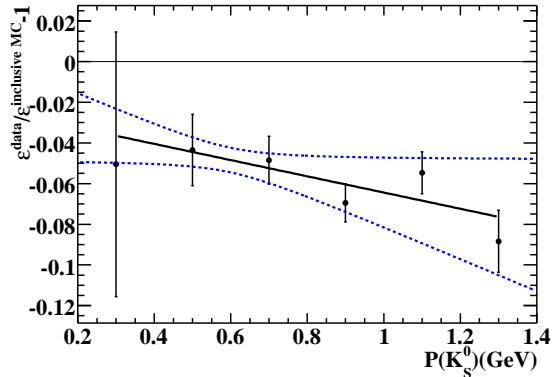

FIG. 4: The difference in the K_S^0 reconstruction efficiency between data and MC simulation (points with error bars), together with the fit to the difference with a linear function of momentum. The solid line is from the best fit and the dashed lines are the $\pm 1\sigma$ envelopes of the best fit.

B.   Kinematic fit

In the MC simulation, the model is much simpler than the real detector performance, and this results in differences between data and MC simulation in the track parameters of photons and charged tracks. The simulation of the photon has been checked in another analysis [10], which shows good agreement between data and MC simulation. For the charged tracks, careful comparisons with purely selected data samples indicate that the MC simulates the momentum and angular resolutions significantly better than those in data, while the error matrix elements agree well between data and MC simulation. This results in a much narrower χ_{4C}^2 distribution in MC than in data, and introduces a bias in the efficiency estimation. We correct the track helix parameters of MC simulation to reduce the difference between data and MC simulation.

We use $J/\psi \to \phi f_0(980)$, $\phi \to K^+ K^-$, $f_0(980) \to \pi^+ \pi^-$ as a control sample to study the difference on the helix parameters of charged tracks between data and MC simulation, as this channel has a large production rate, very low background, and has both pions and

17

kaons. We find that the pull distributions of data are wider than MC simulation and the peak positions are shifted. These obvious differences between data and MC simulation suggest wrong track parameters have been set in MC simulation. The helix parameters of each track in the MC simulation are enlarged by smearing with a Gaussian function $G(\mu, \sigma) = G((\mu_i^{\text{data}} - \mu_i^{\text{MC}}) \times V_{ii}, \sqrt{(\sigma_i^{\text{data}}/\sigma_i^{\text{MC}})^2 - 1} \times V_{ii})$, where $i = \{d\rho, \phi_0, \kappa, dz, tg\lambda\}$ is the i-th helix parameter of the track and V is the corresponding covariance matrix. Here $d\rho$ is the distance from the pivot to the orbit in the x-y plane, ϕ_0 is the azimuthal angle specifies the pivot with respect to the helix center, κ is the reciprocal of the transverse momentum, dz is the distance of the helix from the pivot to the orbit in the z direction, and $tg\lambda$ is the slope of the track. The correction factors μ_i^{data}, μ_i^{MC}, σ_i^{data}, and σ_i^{MC} are the means and resolutions of the pull distributions of the data and MC simulation obtained from control samples, which are listed in Table VI.

After applying the corrections for many final states, we find that the agreement between data and MC simulation does improve significantly but differences still exist. This indicates that the effect is from multiple sources, and our procedure is not a complete solution to the problem. The comparison of $\chi_{4\text{C}}^2$ distributions between data and MC simulation before and after the track-parameter-correction are shown in Figs. 5 and 6 for $\chi_{cJ} \to K_S^0 K^{\pm} \pi^{\mp} \pi^+ \pi^-$ and $K^+ K^- \pi^+ \pi^- \pi^0$, respectively. Doing a χ^2 test between data and MC simulation before and after correction, we find the probability of the agreement changes from 10^{-18} (10^{-3}) level to 10^{-4} (10^{-1}) level for $K_S^0 K^{\pm} \pi^{\mp} \pi^+ \pi^- (K^+ K^- \pi^+ \pi^- \pi^0)$. We take the efficiency from the track-parameter-corrected MC samples as the nominal value, and take half of the difference between MC samples before and after the correction as the systematic error from the kinematic fitting. This is a conservative estimation as the uncertainties of the correction factors are at 10% level and the difference between data and MC simulation in the χ_{4C}^2 distributions after the correction are much smaller than that before doing correction.

The systematic errors in $\mathcal{B}(\chi_{cJ} \to K_S^0 K^{\pm} \pi^{\mp} \pi^+ \pi^-)$ ($\mathcal{B}(\chi_{cJ} \to K^+ K^- \pi^+ \pi^- \pi^0)$) are 1.5%, 1.9%, and 1.7% (0.4%, 0.4%, and 0.2%) for $J = 0$, 1, and 2, respectively; and 1.5%, 1.7%, and 1.8% (0.9%, 0.2%, and 0.4%) systematic uncertainties are assigned to $\mathcal{B}(\chi_{cJ} \to \eta_c \pi^+ \pi^-)$ with $\eta_c \to K_S^0 K^{\pm} \pi^{\mp}$ ($K^+ K^- \pi^0$) for $J = 0$, 1, and 2, respectively.

TABLE VI: Correction factors extracted from pull distributions using a control sample of $J/\psi \rightarrow \phi f_0(980)$, $\phi \rightarrow K^+K^-$, $f_0(980) \rightarrow \pi^+\pi^-$.

	ϕ_0		κ		$tg\lambda$	
	$\mu^{\text{data}} - \mu^{\text{MC}}$	$\sigma^{\text{data}}/\sigma^{\text{MC}}$	$\mu^{\text{data}} - \mu^{\text{MC}}$	$\sigma^{\text{data}}/\sigma^{\text{MC}}$	$\mu^{\text{data}} - \mu^{\text{MC}}$	$\sigma^{\text{data}}/\sigma^{\text{MC}}$
K^+	-0.04 ± 0.03	1.19 ± 0.02	-0.24 ± 0.03	1.28 ± 0.02	-0.38 ± 0.01	1.25 ± 0.02
K^-	0.06 ± 0.03	1.21 ± 0.02	0.25 ± 0.03	1.25 ± 0.02	-0.36 ± 0.01	1.21 ± 0.02
π^+	-0.06 ± 0.03	1.25 ± 0.02	-0.10 ± 0.03	1.31 ± 0.02	-0.36 ± 0.01	1.25 ± 0.02
π^-	-0.02 ± 0.03	1.23 ± 0.02	0.10 ± 0.03	1.27 ± 0.02	-0.36 ± 0.01	1.21 ± 0.02

C. Uncertainty from damping factor

In the fit to the invariant mass spectrum of $K_S^0 K^\pm \pi^\mp \pi^+ \pi^-$ and $K^+ K^- \pi^+ \pi^- \pi^0$, the damping function used by KEDR is adopted. Another damping factor used by CLEO [22] is $e^{-E_\gamma^2/8\beta^2}$ with $\beta = (0.0650 \pm 0.0025)$ GeV determined from their fit. Using this damping function with $\beta = (0.097 \pm 0.024)$ GeV which is extracted from fitting χ_{c0} data, the differences on the branching fractions of $\chi_{cJ} \rightarrow K_S^0 K^\pm \pi^\mp \pi^+ \pi^-$ ($\chi_{cJ} \rightarrow K^+ K^- \pi^+ \pi^- \pi^0$) are assigned to the systematic error due to damping function, which are 0.5%, 0.1%, and 0.1% (0.4%, 0.1%, and 0.1%) for $J = 0$, 1, and 2, respectively. The effect for χ_{c1} and χ_{c2} is small since the two states are very narrow.

D. Uncertainty from intermediate states

The detection efficiencies for the measurement of $\mathcal{B}(\chi_{cJ} \rightarrow K_S^0 K^\pm \pi^\mp \pi^+ \pi^-)$ and $\mathcal{B}(\chi_{cJ} \rightarrow K^+ K^- \pi^+ \pi^- \pi^0)$ are estimated using the MC simulation with χ_{cJ} decay to $K_S^0 K^\pm \pi^\mp \pi^+ \pi^-$ and $K^+ K^- \pi^+ \pi^- \pi^0$ generated according to pure phase space distribution. From the data, we see broad intermediate states such as K^* and ρ in the invariant mass spectra of $K\pi$ and $\pi\pi$. The branching fractions of $\chi_{cJ} \rightarrow K_S^0 K^\pm \pi^\mp \pi^+ \pi^-$ ($\chi_{cJ} \rightarrow K^+ K^- \pi^+ \pi^- \pi^0$) via these intermediate states are measured by fitting the invariant mass spectra of $K\pi$ and $\pi\pi$. An alternative signal MC sample is generated with all possible intermediate states and corresponding branching fractions to determine the efficiency. The efficiency difference between this sample and the phase space sample is about 1.0% for $\chi_{cJ} \rightarrow K_S^0 K^\pm \pi^\mp \pi^+ \pi^-$ and
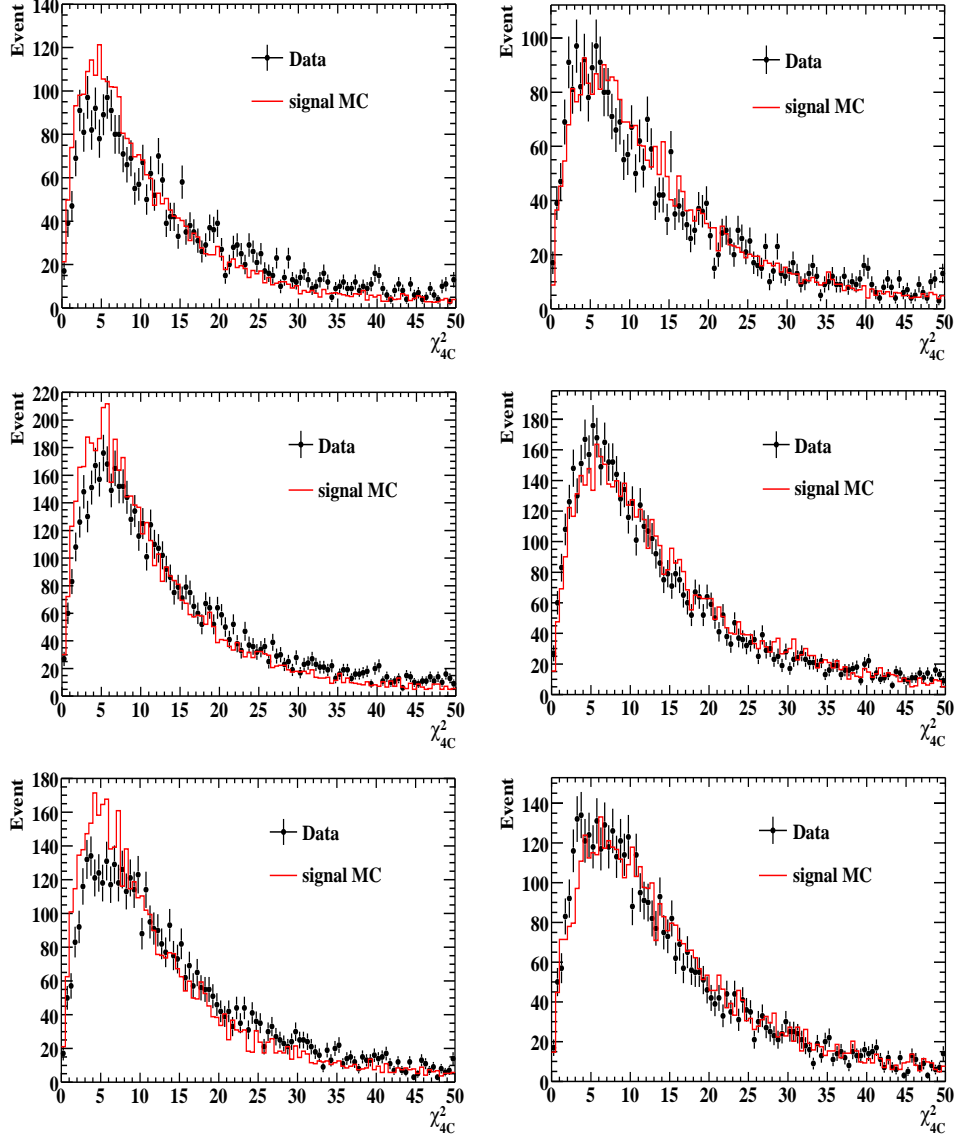
FIG. 5: Comparison of χ^2_{4C} between signal MC and data for $\psi(3686) \rightarrow \gamma\chi_{cJ}$, $\chi_{cJ} \rightarrow K^0_S K^{\pm}\pi^{\mp}\pi^{+}\pi^{-}$. The points with error bars are data, and the solid lines are MC simulation. Left panel: signal MC without track-parameter-correction; Right panel: signal MC after track-parameter-correction. From top to bottom are χ_{c0}, χ_{c1}, and χ_{c2}, respectively.

4.0% for $\chi_{cJ} \rightarrow K^+K^-\pi^+\pi^-\pi^0$; these are taken as the systematic error due to intermediate states.
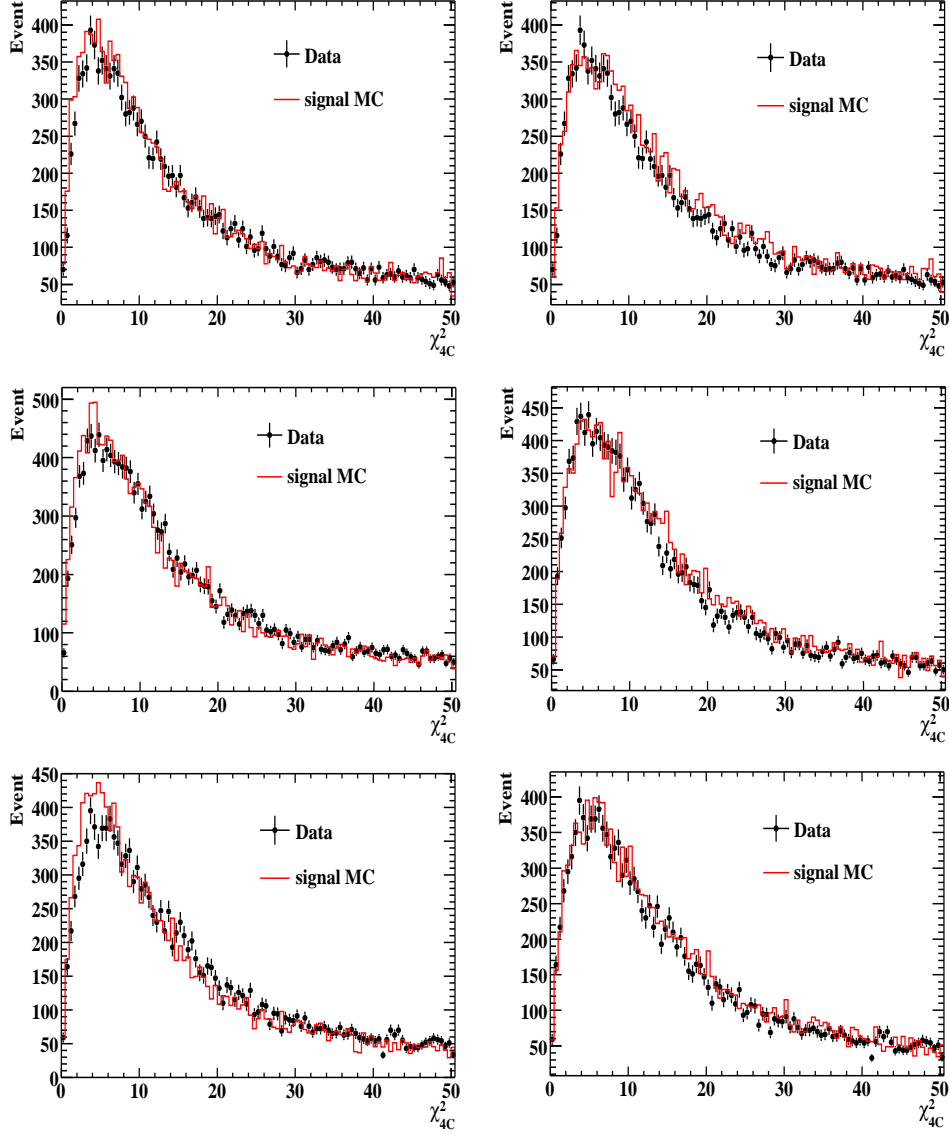
FIG. 6: Comparison of χ^2_{4C} between signal MC and data for $\psi(3686) \rightarrow \gamma\chi_{cJ}$, $\chi_{cJ} \rightarrow K^+K^-\pi^+\pi^-\pi^0$. The points with error bars are data, and the solid lines are signal MC plus possible background estimated using inclusive MC sample. Left panel: signal MC without track-parameter-correction; Right panel: signal MC after track-parameter-correction. From top to bottom are χ_{c0}, χ_{c1}, and χ_{c2}, respectively.

E. Uncertainty from fitting

In the measurement of $\mathcal{B}(\chi_{cJ} \rightarrow K\bar{K}\pi\pi)$, the systematic uncertainty due to the fitting range is estimated by fitting the invariant mass spectrum in the range [3.25, 3.61] GeV/c^2

and [3.35, 3.60] GeV/c^2. The biggest differences in the branching fractions are assigned as errors, which are 1.0%, 0.4%, and 0.2% for χ_{c0}, χ_{c1}, and χ_{c2}, respectively, in $K^0_S K^\pm \pi^\mp \pi^+ \pi^-$ decay; and 0.4%, 0.4%, and 0.7% for χ_{c0}, χ_{c1}, and χ_{c2}, respectively, in $K^+ K^- \pi^+ \pi^- \pi^0$ decay. The background shape is changed from a second-order Chebyshev polynomial to a third-order Chebyshev polynomial, and the differences are taken to be the systematic errors, which are 1.4%, 0.7%, and 0.6% for χ_{c0}, χ_{c1}, and χ_{c2}, respectively, in $K^0_S K^\pm \pi^\mp \pi^+ \pi^-$; and 1.3%, 0.7%, and 0.4% for χ_{c0}, χ_{c1}, and χ_{c2} in $K^+ K^- \pi^+ \pi^- \pi^0$.

In the measurement of $\mathcal{B}(\chi_{cJ} \to \eta_c \pi^+ \pi^-)$, for each decay mode in the three χ_{cJ} states, the fit-related systematic errors on the signal yield are estimated by changing the fit ranges, the orders of the background polynomial, the detector resolutions (resolution from MC simulation directly or from MC simulation convolved with a Gaussian accounts for the difference between data and MC simulation, the sigma of the Gaussian is fixed to the resolution difference found in the χ_{cJ} signals measured in Sect. IV A), and the η_c line shapes with the parameters of η_c varied by one standard deviation [17]; the maximum N^{up} is used in the upper limit calculation.

VI. RESULTS AND DISCUSSION

Using the numbers of signal χ_{cJ} events from the fits, together with the corresponding efficiencies, the branching fractions of $\chi_{cJ} \to K^0_S K^\pm \pi^\mp \pi^+ \pi^-$ ($\chi_{cJ} \to K^+ K^- \pi^+ \pi^- \pi^0$) are determined and listed in Table VII. In the measurement of the branching fractions of $\chi_{cJ} \to K^+ K^- \pi^+ \pi^- \pi^0$, contributions from narrow resonances η, ω, and ϕ are subtracted. We measure for the first time the branching fractions of $\chi_{cJ} \to K^0_S K^\pm \pi^\mp \pi^+ \pi^-$ and $\chi_{cJ} \to K^+ K^- \pi^+ \pi^- \pi^0$. Comparing the two decay modes, we find that the ratio of the branching fractions is around one-half which may be a consequence of isospin symmetry. We also measured the branching fractions of $\chi_{cJ} \to \omega K^+ K^-$ and $\chi_{cJ} \to \phi \pi^+ \pi^- \pi^0$ for the first time, the results are listed in Table VII as well.

The upper limits on the branching fraction of $\chi_{cJ} \to \eta_c \pi^+ \pi^-$ in the two decay modes are listed in Table VIII. After the peaking background subtraction, there is an about 2σ excess in the $\chi_{c2} \to \eta_c \pi^+ \pi^-$. We give a more stringent constraint on the $\chi_{c2} \to \eta_c \pi^+ \pi^-$ branching fraction than BaBar does [8]. The decay $\chi_{c0} \to \eta_c \pi^+ \pi^-$ is forbidden by spin-parity conservation, thus the measurement on η_c signals in the χ_{c0} mass region gives an access to the

TABLE VII: The results for $\mathcal{B}(\chi_{cJ} \to K_S^0 K^\pm \pi^\mp \pi^+ \pi^-)$, $\mathcal{B}(\chi_{cJ} \to K^+ K^- \pi^+ \pi^- \pi^0)$, $\mathcal{B}(\chi_{cJ} \to \omega K^+ K^-)$, and $\mathcal{B}(\chi_{cJ} \to \phi \pi^+ \pi^- \pi^0)$. The first errors are statistical and the second ones are systematic.

Decay mode	N^{signal}	ϵ (%)	$\mathcal{B}$ ($\times 10^{-3}$)
$\chi_{c0} \to K_S^0 K^\pm \pi^\mp \pi^+ \pi^-$	2789 ± 66	9.30	$4.22 \pm 0.10 \pm 0.43$
$\chi_{c0} \to K^+ K^- \pi^+ \pi^- \pi^0$	9031 ± 132	10.34	$8.61 \pm 0.13 \pm 0.94$
$\chi_{c0} \to \omega K^+ K^-$	1414 ± 42	8.04	$1.94 \pm 0.06 \pm 0.20$
$\chi_{c0} \to \phi \pi^+ \pi^- \pi^0$	538 ± 29	9.16	$1.18 \pm 0.07 \pm 0.13$
$\chi_{c1} \to K_S^0 K^\pm \pi^\mp \pi^+ \pi^-$	5180 ± 75	10.21	$7.52 \pm 0.11 \pm 0.79$
$\chi_{c1} \to K^+ K^- \pi^+ \pi^- \pi^0$	12256 ± 127	11.10	$11.46 \pm 0.12 \pm 1.29$
$\chi_{c1} \to \omega K^+ K^-$	628 ± 29	9.34	$0.78 \pm 0.04 \pm 0.08$
$\chi_{c1} \to \phi \pi^+ \pi^- \pi^0$	373 ± 26	10.50	$0.75 \pm 0.06 \pm 0.08$
$\chi_{c2} \to K_S^0 K^\pm \pi^\mp \pi^+ \pi^-$	4559 ± 71	9.76	$7.30 \pm 0.11 \pm 0.75$
$\chi_{c2} \to K^+ K^- \pi^+ \pi^- \pi^0$	11189 ± 124	10.48	$11.69 \pm 0.13 \pm 1.31$
$\chi_{c2} \to \omega K^+ K^-$	512 ± 27	8.58	$0.73 \pm 0.04 \pm 0.08$
$\chi_{c2} \to \phi \pi^+ \pi^- \pi^0$	408 ± 28	9.88	$0.93 \pm 0.06 \pm 0.10$

possible direct production of $\psi(3686) \to \gamma \eta_c \pi^+ \pi^-$, which is not significant in our data and is neglected in the analysis, and thus our upper limits on the $\chi_{cJ} \to \eta_c \pi^+ \pi^-$ are conservative. The theoretical prediction of $\mathcal{B}(\chi_{c1} \to \eta_c \pi^+ \pi^-)$ is also listed in Table VIII, which is larger than our measurements. We note that the theoretical prediction uses experimental results as input to normalize the parameters in the model. For example, the parameter α_M/α_E is extracted by comparing the branching fraction of $\psi(3686) \to h_c \pi^0$ between the theoretical calculation and the experimental measurement. This makes the prediction highly dependent on the former experimental results and theoretical models. This may partly explain the discrepancy between the theoretical prediction and the experimental results.

TABLE VIII: Upper limits at the 90% C.L. on $\mathcal{B}(\chi_{cJ} \to \eta_c \pi^+ \pi^-)$ in the two η_c decay modes. N^{fit} is the number of events from the fits shown in Fig.3, N^{signal} is the number of events after the peaking background subtraction, $N^{\text{up}}_{\text{observed}}$ is the upper limit on the number of events at the 90% C.L. observed on data, and $N^{\text{up}}_{\text{expected}}$ is the expected upper limit on the number of events at the 90% C.L. from toy MC experiments. In the χ_{c2} case, N^{fit} includes the contribution from the peaking background $\psi(3686) \to \pi^+ \pi^- J/\psi, J/\psi \to \gamma \eta_c, \eta_c \to K^0_S K^\pm \pi^\mp (K^+ K^- \pi^0)$.

Decay mode	N^{fit}	N^{signal}	$N^{\text{up}}_{\text{observed}}$	$N^{\text{up}}_{\text{expected}}$	ϵ (%)	$\mathcal{B}^{\text{up}}(\chi_{cJ} \to \eta_c \pi^+ \pi^-)$ (%)	$\mathcal{B}^{\text{theory}}(\chi_{cJ} \to \eta_c \pi^+ \pi^-)$ (%)
$\chi_{c0} \to (K^0_S K^\pm \pi^\mp)\pi^+ \pi^-$	0.0 ± 4.6	0.0 ± 4.6	6.8	7.1	6.29	0.07	-
$\chi_{c0} \to (K^+ K^- \pi^0)\pi^+ \pi^-$	0 ± 15	0 ± 15	34	27	6.82	0.41	-
$\chi_{c1} \to (K^0_S K^\pm \pi^\mp)\pi^+ \pi^-$	18 ± 17	18 ± 17	49	44	9.45	0.32	1.81 ± 0.26
$\chi_{c1} \to (K^+ K^- \pi^0)\pi^+ \pi^-$	6 ± 25	6 ± 25	50	47	9.82	0.44	
$\chi_{c2} \to (K^0_S K^\pm \pi^\mp)\pi^+ \pi^-$	77 ± 19	31 ± 22	64	63	7.72	0.54	-
$\chi_{c2} \to (K^+ K^- \pi^0)\pi^+ \pi^-$	89 ± 26	55 ± 27	105	94	7.83	1.2	-

[1] N. Brambilla *et al.* (Quarkonium Working Group), CERN Yellow Report, CERN-2005-005.

[2] N. Brambilla *et al.* (Quarkonium Working Group), Eur. Phys. J. C **71**, 1534 (2011).

[3] T. M. Yan, Phys. Rev. D **22**, 1652 (1980).

[4] Y.-P. Kuang, S. F. Tuan, and T. M. Yan, Phys. Rev. D **37**, 1210 (1988).

[5] Y.-P. Kuang and T.-M. Yan, Phys. Rev. D **24**, 2874 (1981).

[6] Y.-P. Kuang, Front. Phys China **1**, 19 (2006).

[7] C. Cawlfield *et al.* (CLEO Collaboration), Phys. Rev. D **73**, 012003 (2006).

[8] J. P. Lees *et al.* (BaBar Collaboration), arXiv:1206.2008 [hep-ex].

[9] Q. Lu and Y.-P. Kuang, Phys. Rev. D **75**, 054019 (2007). The predicted branching fraction is recalculated with the parameters in the model determined using the updated expermential data: $\Gamma(\psi(3686)) = (304\pm9)$ keV, $\mathcal{B}(\psi(3686) \to J/\psi\pi\pi) = (51.35\pm0.52)\%$, and $\mathcal{B}(\psi(3686) \to h_c\pi^0) \times \mathcal{B}(h_c \to \gamma\eta_c) = (4.35 \pm 0.57) \times 10^{-4}$. The total width of $\psi(3686)$ and the branching fraction of $\psi(3686) \to J/\psi\pi\pi$ are taken from PDG, while the $\mathcal{B}(\psi(3686) \to h_c\pi^0) \times \mathcal{B}(h_c \to \gamma\eta_c)$ is the combined result from the measurement in CLEO and BESIII Collaboration.

[10] M. Ablikim *et al.* (BESIII Collaboration), Phys. Rev. D **81**, 052005 (2010).

[11] M. Ablikim *et al.* (BESIII Collaboration), Nucl. Instrum. Meth. A **614**, 345 (2010).

[12] S. Agostinelli *et al.* (GEANT4 Collaboration), Nucl. Instrum. Meth. A **506**, 250 (2003).

[13] S. Jadach, B. F. L. Ward and Z. Was, Comp. Phys. Commu. **130**, 260 (2000); Phys. Rev. D **63**, 113009 (2001).

[14] http://www.slac.stanford.edu/~lange/EvtGen/; R. G. Ping *et al.*, Chinese Physics C **32**, 599 (2008).

[15] J. Beringer *et al.*, Phys. Rev. D **86**, 010001 (2012).

[16] J. C. Chen, G. S. Huang, X. R. Qi, D. H. Zhang and Y. S. Zhu, Phys. Rev. D **62**, 034003 (2000).

[17] M. Ablikim *et al.* (BESIII Collaboration), Phys. Rev. Lett. **108**, 222002 (2012).

[18] V. V. Anashin *et al.*, arXiv:1012.1694 [hep-ex].

[19] M. Ablikim *et al.* (BESIII Collaboration), Phys. Rev. Lett. **107**, 092001 (2011).

[20] M. Ablikim *et al.* (BESIII Collaboration), Phys. Rev. Lett. **105**, 261801 (2010).

[21] M. Ablikim *et al.* (BESIII Collaboration), Phys. Rev. D **83**, 112005 (2011).

[22] R. E. Mitchell *et al.* (CLEO Collaboration), Phys. Rev. Lett. **102**, 011801 (2009).